2-bit reconfigurable unit-cell and electronically steerable transmitarray at Ka-band

Fatimata Diaby, Antonio Clemente, Ronan Sauleau, Trung Kien Pham, Laurent Dussopt

2-Bit Reconfigurable Unit-Cell and Electronically Steerable Transmitarray at Ka-Band

Fatimata Diaby, Antonio Clemente, *Senior Member, IEEE,* Ronan Sauleau, *Fellow, IEEE*, Kien T. Pham, *Member, IEEE,* and Laurent Dussopt, *Senior Member, IEEE*

***Abstract*—This paper presents the design, optimization, fabrication, and characterization of an electronically steerable transmitarray with 2 bits of phase quantization per unit cell. The proposed transmitarray operates in linear polarization at Ka-band and is composed of 14×14 reconfigurable unit-cells. Four p-i-n diodes are integrated on each unit-cell to control the radiated field phase distribution across the transmitarray aperture. The prototype demonstrates experimentally pencil beam scanning over a 120×120-degree window, a maximum gain at broadside of 19.8 dBi, and a 3-dB fractional bandwidth of 16.2%.**

***Index Terms*—Transmitarray antennas, beam steering, beam forming, Ka-band, discrete lens, electronically steerable antenna.**

I. Introduction

The demonstration of relatively low-cost and innovative antenna technologies for user terminals with electronically beam-steering capabilities is a key element in the development of the future Internet of Space (IoS) ecosystem [1]. This innovative communication network will deliver high data-rate services to every part of the globe thanks to future-generation terrestrial and broadband satellite networks.

Satellite constellations operating at Ka-band play a fundamental role to increase the system bandwidth and consequently the achievable data rate; the allocated frequency bands for both military and civil applications are 17.7 – 21.2 GHz and 27.5 – 31.0 GHz, for the downlink and uplink respectively. In the last years, several antenna configurations based on fully mechanical (e.g. [2],[3]), hybrid electromechanical (e.g. [4]), and electronically steerable (e.g. [5]-[7]) architectures have been presented as academic or industrial solutions. The existing fully electronically reconfigurable architectures are based on liquid crystal controlled holographic metasurfaces [5],[6] or more importantly on classical phased arrays, e.g. [7].

For the future 5th Generation mobile terrestrial networks, several frequency ranges (24.27 – 27.5 GHz, 31.8 – 33.4 GHz, or 37.0 – 40.5 GHz) at Ka-band have been indicated as potential candidates for the development of high performance backhauling and access point systems [8]. In the last years, several phased array solutions [9] have been proposed and are generally based on analogue [10] or fully-digital architectures [11].

Thanks to their spatial feeding architecture and the possibility to control easily the phase distribution on the array aperture, transmitarrays (TAs) and reflectarrays are excellent alternatives for beam steerable applications. In contrast to reflectarrays, TAs do not suffer from any feed blockage. Moreover, advanced TA designs may lead to ultra-low profile architectures [12]-[13] and to a full control of the transmission phase and polarization at the same time [14]. A TA is typically composed of one or several focal sources illuminating an array of unit-cells (flat lens). Each unit-cell consists of a first antenna array working in receive mode and connected (through phase shifters) to a second array working in transmission mode.

Several wideband fixed- [14]-[15] or switched-beam [16], and electronically-reconfigurable TAs [12],[13],[17]-[20] have been presented and demonstrated in the literature up to sub-THz frequencies [21]. In our previous works [12],[18], the possibility to implement electronic beam-scanning has been successfully shown using 1-bit reconfigurable TAs with 800 p-i-n diodes integrated on the antenna aperture. Shaped beams (*e.g.* flat-top patterns) have also been demonstrated [18]. One-bit architectures are relatively low cost, low loss, and wideband (3-dB gain bandwidth up to 15%) due to reduced number of layers and solid-state devices integrated to control the transmission phase. However, the limited phase resolution leads to directivity loss (close to 4 dB for a 400-element antenna) and high side lobes. Two-bit phase quantization can be used to increase both aperture efficiency and radiation pattern quality at the cost of a higher complexity and optimization constraints.

Here a 2-bit electronically-reconfigurable TA prototype is presented at Ka-band. The proposed antenna is based on the reconfigurable unit-cell architecture previously reported in our preliminary conference works [22],[23]. To the best of our knowledge, the TA prototype described here is one of the largest (14×14 unit-cells) 2-bit electronically-reconfigurable TA presented in the open literature at Ka-band, and its radiation efficiency is among the highest reported so far (around 48%). The only 2-bit prototype previously introduced in [17] contains 22×22 unit-cells, but the radiation characteristics demonstrated experimentally were degraded by the low reliability of the MEMS technology used (about 8 dB gain reduction).

This paper is organized as follows. The architectures of the proposed 2-bit electronically reconfigurable unit-cell and TA and the fabricated prototypes are presented in Section II. Then, we describe in Section III the radiation performance obtained in simulations and measurements. Finally, conclusion are drawn in Section IV.

II. Transmitarray Architecture, Design and Fabrication

A. 2-Bit Reconfigurable Unit-Cell: Design, Fabrication and Experimental Characterization

The global architecture, details on geometrical parameters, operation principle, and numerical analysis of the 2-bit reconfigurable unit-cell have been described and discussed in [22],[23]. Standard Printed Circuit Board (PCB) process, *i.e.* with minimum trace width of 80 µm and minimum via-diameter of 120 µm, has been selected to demonstrate the possibility to implement the proposed design by using mature and relatively low cost fabrication technologies. This unit-cell

Manuscript received December 19, 2018, revised July 30, 2019, accepted November 17, 2019. This work was supported by the National Research Agency through the project "TRANSMIL" under Grant ANR-14-CE28-0023.

F. Diaby, A. Clemente, and L. Dussopt are with CEA-LETI, Minatec Campus, F38054 Grenoble, France (e-mail: antonio.clemente@cea.fr).

R. Sauleau is with Univ Rennes, CNRS, IETR (Institut d'Électronique et de Télécommunications de Rennes), UMR 6164, F-35000 Rennes, France (e-mail: ronan.sauleau@univ-rennes1.fr).

K. T. Pham was with Univ Rennes, CNRS, IETR (Institut d'Électronique et de Télécommunications de Rennes), UMR 6164, F-35000 Rennes, France. He is now with International Univ. VNU-HCM, Ho Chi Minh City, Vietnam.

(see its cross section view in Fig. 1(a)) has a size of 5.1×5.1×1.3 mm^3 ($\lambda_0/2\times\lambda_0/2\times\lambda_0/8$ at 29 GHz, where λ_0 is the wavelength in free space at this frequency). It is fabricated on three Rogers RT/Duroid 6002 substrates (ε_r = 2.94, tanδ = 0.0012) bonded with two RO4450F films (ε_r = 3.52, tanδ = 0.004). The selected substrates have been previously used in our passive design at Ka-band [14], showing the possibility to achieve transmission loss lower than 1-dB on a bandwidth in the range 10 – 15%. Compared to the dielectric stack-up used in [22],[23], it is important to notice that a new bonding film has been used here to improve the mechanical stability and fabrication yield of this multilayer PCB stack-up. Therefore, the geometrical parameters of the unit-cell have been re-optimized to take into account this new configuration.

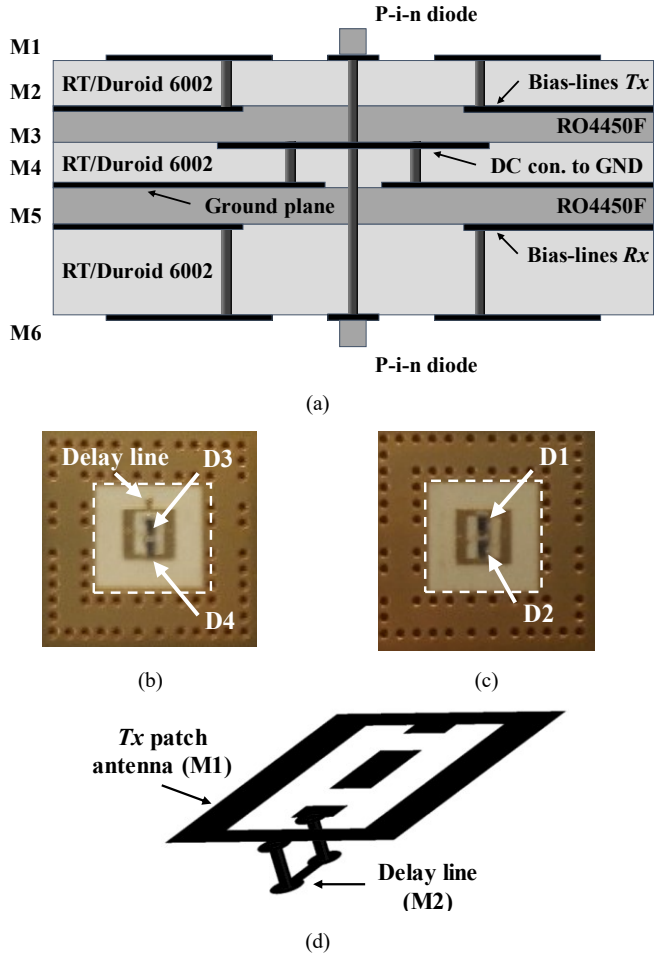

Fig. 1. Reconfigurable 2-bit unit-cell. (a) Cross-section view. Photographs of the realized prototype: (b) transmitting (*Tx*) patch printed on metal layer M1, and (c) receiving (*Rx*) patch printed on M6. (d) Schematic view of the delay line connected to the *Tx* patch antenna. P.-i.-n. diodes are labeled D1 to D4 in (b) and (c).

The radiating elements consist of center-fed O-slot rectangular patch antennas working in transmitting (*Tx*, Fig. 1(b)) and in receiving (*Rx*, Fig. 1(c)) modes, respectively. These two patch antennas are printed on the top (M1) and bottom (M6) metal layers of the dielectric stack-up and are connected by a metalized thru via hole (diameter: 200 µm) located at their center. A ground plane printed on M4 separates and isolates both patches. Two p-i-n diodes MA4GFCP907 [24] are flip-chipped on each patch antenna to tune the transmission phase with a 2-bit quantization (*i.e.* four phase states with a 90° relative phase shift); they are controlled by two bias lines printed on the opposite side (layers M2 and M5) of each patch substrate. The bias network includes microstrip radial stubs and capacitors to isolate the RF signals in *Tx* and *Rx* sides, respectively. The DC connection to ground is realized with a short circuit stub (M3) and connected to the ground plane by using metallized vias (from M3 to M4). The bias lines are also connected to the patches by metallized vias (from M1 to M2, and from M5 to M6).

In our design, p-i-n diodes are used to limit the number of the bias lines (*i.e.* only two lines to correctly bias four devices) and achieve relatively low insertion loss compared to other technologies, such as varactor diodes [13] (3.2 dB at 4.8 GHz) or MEMS switches [17] (in the range 4.9 – 9.2 dB as a function of the phase state at 38.8 GHz).

The unit-cell has been designed using Ansys HFSS, version 18. The p-i-n diodes are modeled by lumped-elements equivalent circuits valid up to 40 GHz; this model, previously extracted from on-PCB measurements [25], consists of a series circuit (R_{ON} = 4.2 Ω, L_{ON} = 0.05 nH) and a shunt circuit (R_{OFF} = 300 kΩ, C_{OFF} = 42 fF), in the forward (I_{bias} = 10 mA) and reverse (V_{bias} = 1.2 V) state, respectively.

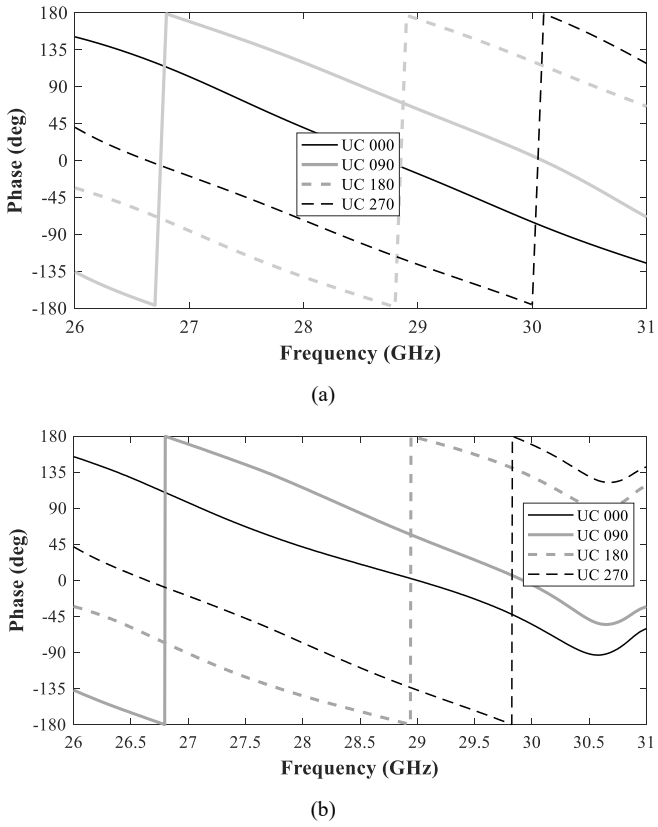

Fig. 2. (a) Simulated and (b) measured transmission phase of the four phase states of the proposed unit-cell.

The complete operation principle of this unit-cell, including the analysis of the surface current distributions on both patch antennas has been detailed in [23] as a function of the p-i-n diode states. For completeness, a summary is reported here. Both p-i-n diodes on each radiating element are biased in opposite states (when one diode is switched ON, the other one is in OFF state, and *vice versa*). More precisely, switching between D1 and D2 (Fig. 1(c)) leads to an inversion of the surface-current flow on the *Rx* metal layer. As a result, a 180° phase-shift is achieved on the *Rx* patch antenna, as in the case of the 1-bit unit-cell introduced in [25]. The same mechanism is employed on the *Tx* metal layer by switching the p-i-n diodes D3 and D4 (Fig. 1(b)). Moreover, an additional phase-shift close to 90° is obtained on the *Tx* patch antenna (M1) thanks to the delay line printed

on M2 (Fig. 1(d)) and connected to the rectangular patch (M1). As a result, four phase states are obtained: 0°, 90°, 180° and 270°.

The fabricated unit-cell (labelled UC000, UC090, UC180, and UC270) has been characterized using the waveguide simulator described in [25] (*i.e.* two rectangular waveguides WR-28 and two rectangular-to-square waveguide transitions). As shown in Fig. 1(b)-(c), two rings of vias and a large ground plane are used to guarantee a good electrical contact between the waveguide flanges and the unit-cell prototypes. Furthermore, the simulated results have been obtained by modeling the waveguide setup used experimentally. The simulated 3-dB absolute transmission bandwidth (BW) is equal to 9.6%, 16.5%, 12.1% and 15.5% for UC000, UC090, UC180, and UC270, respectively. They are in acceptable agreement with the measured values (11.7%, 10.1%, 12.1%, and 10.3%, respectively).

The simulated and measured transmission phase of the unit-cell is plotted in Fig. 2 for the four phase-states. The measured relative phase-shift between the UC000 state and the three other states (UC090, UC180, and UC270) is equal to 124°, 178°, and 315° at 29 GHz, respectively (in simulation, these values are equal to 105.9°, 178.5°, and 297.6°). The relative phase shift between UC000 and UC180, and between UC090 and UC270, is very stable and nearly equal to 180° over the full unit-cell transmission bandwidth; this comes from the switching mechanism of each pair of diodes, as described above. This result is in agreement with our previous demonstrations [25]. Moreover, the non-perfect 90° phase-shift at central frequency between UC000 and UC090, and between UC180 and UC270, is due to the complexity of the optimization and to the standard PCB fabrication constraints considered in the design.

The differences between the simulated and measured results are most probably due to the misalignment of the unit-cell in the waveguide setup and to the PCB fabrication errors (layer misalignments, geometrical dimensions, non-uniform thickness of the bonding film layers due to the pressing process, etc.). These statements have been confirmed by retro-simulations, but the detailed presentation of the results is out of the scope of this paper. The insertion loss measured and simulated at 29 GHz and the 3-dB transmission bandwidth of the unit-cell in the four phase-states are summarized in Table I.

TABLE I
MEASURED AND SIMULATED PERFORMANCE OF THE 2-BIT UNIT-CELL

	Transm. loss at 29 GHz (dB)		3-dB transm. BW (GHz)		Phase shift at 29 GHz (deg.)	
	Sim.	**Meas.**	**Sim.**	**Meas.**	**Sim.**	**Meas.**
UC000	1.0	2.1	27.0 – 30.1	26.8 – 30.2	-	-
UC090	0.8	1.5	27.4 – 31.0	27.4 – 30.3	105.9	124.0
UC180	1.0	2.3	26.8 – 30.5	26.7 – 30.2	178.5	178.0
UC270	0.8	1.6	27.5 – 31.3	27.3 – 30.3	297.6	315.0

B. Transmitarray Design and Fabrication

The fabricated 14×14-element TA is shown in Fig. 3. The aperture size has been chosen to achieve similar performance (i.e. gain in the range of 20 – 23 dBi) if compared to the one of our previous works at Ka-band [12]. The flat panel (142×163 mm²) is realized on the same dielectric stack-up as for the unit-cell (Fig. 1(a)). It includes the radiating aperture of size 71.4×71.4 mm² ($7\lambda_0 \times 7\lambda_0$), the 784 p-i-n diodes integrated on the receiving (Fig. 3(a)-(b)) and transmitting layers (Fig. 3(c)-(d)), the DC bias network, and the board-to-board connectors used to interconnect the steering logic. The focal source is a linearly-polarized pyramidal standard gain horn antenna with a nominal gain of 10-dBi. The focal distance is fixed to 48 mm (F/D = 0.67) and has been optimized with our *in-house* tool in order to maximize the aperture efficiency.

C. Bias Network Design and Impact on the Unit-Cell Performance

The fabricated TA is divided into four 7×7 subarrays to bias the 784 integrated p-i-n diodes. Each steering-logic board drives one subarray with two ±10 mA bias currents (one for diodes D1 and D2, and one for D3 and D4) per unit-cell. Considering the p-i-n diode threshold voltage (1.2 V), the total power consumption is 24 mW for each unit-cell and 4.7 W for the full array.

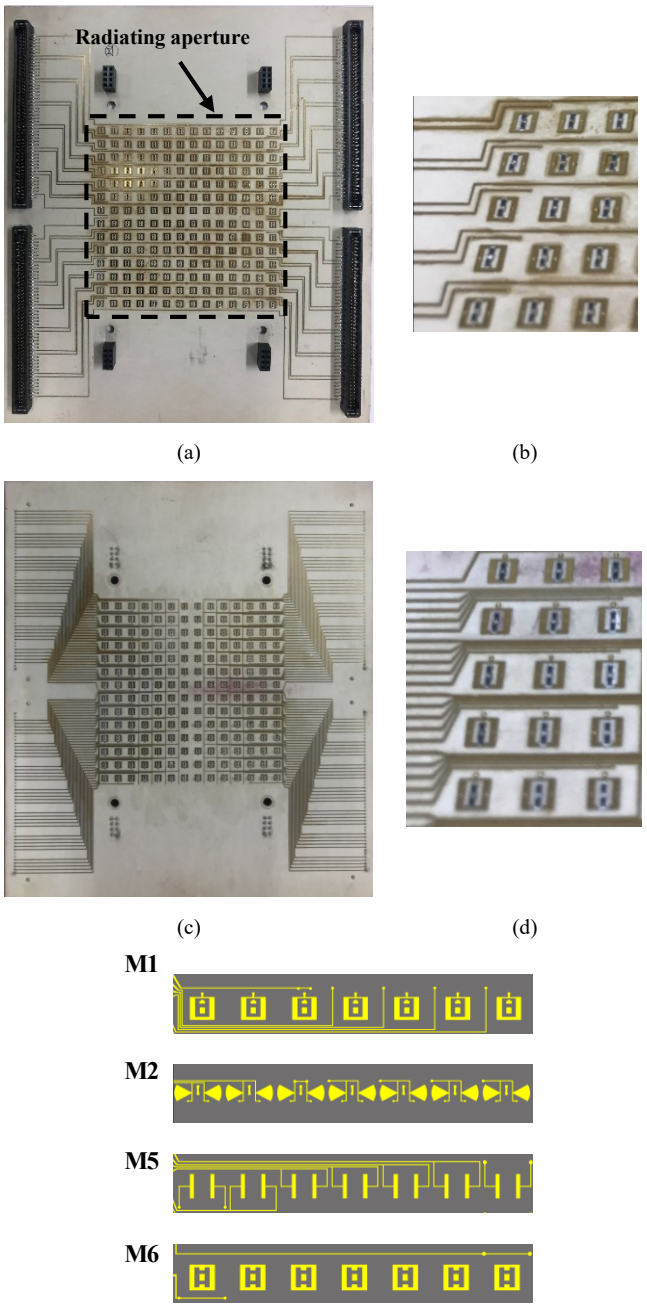

Fig. 3. Photographs of the realized electronically steerable transmitarray, (a)-(b) receiving and (c)-(d) transmitting layers with p-i-n diodes. (e) Schematic view of the bias network on one line of the 7×7 subarray.

The bias lines arrangement is realized by symmetries in both receiving and transmission subarray sides. A total number of 98 bias lines (i.e. two lines per unit-cell) is necessary to bias the 196 p-i-n diodes located on the transmitting and receiving layers of each subarray. The photographs of the TA receiving (M1) and transmitting (M6) layers with their bias line distribution network are shown in Fig. 3(a)-(b) and (c)-(d), respectively. This bias line arrangement is identical for each of the four subarrays. As presented in Fig. 3(e), the bias lines of the transmitting patch diodes are distributed between the layers M1 (5 lines) and M2 (2 lines). On the receiving side, the 7 bias lines have been distributed on layers M5 (5 lines) and M6 (2 lines).

In the proposed analysis, three unit-cell configurations with 2, 6, and 14 DC bias lines have been considered to study the impact of the bias network on the unit-cell frequency response. These three configurations are considered as representative test cases. In the first case, the bias lines controlling the p-i-n diodes soldered on the patch antennas on M1 and M6 are printed on M2 and M5, respectively, as described in the Section II.A. Furthermore, for the configuration with 14 lines, the bias lines are distributed on metallic layers M1, M2, M5 and M6.

These three unit-cell configurations have been simulated with HFSS for the four phase states with periodic conditions and Floquet mode excitation under normal incidence. For brevity purposes, we provide here only experimental results obtained for phase state UC000. The corresponding results (measured amplitude and phase in transmission) are plotted in Fig. 4. The obtained results show very stable scattering parameters in all cases, demonstrating thereby that the DC bias lines do not impact the RF performance, as previously shown in [12],[18]. The impact of the oblique incidence has also been investigated, but the results are not detailed here because the conclusions are the same of the one presented in [18].

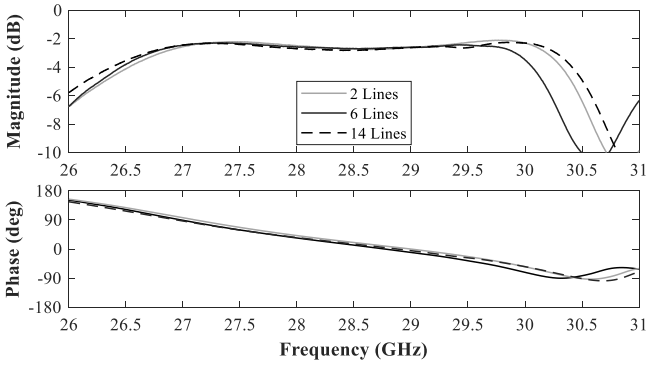

Fig. 4. Measured (a) amplitude and (b) phase of the transmission coefficient of cell UC000 as a function of the frequency and the number of bias lines.

III. Beam Collimating and Scanning: Numerical and Experimental Results

The radiation characteristics of the proposed TA have been computed using our hybrid *in-house* tool based on analytical equations and full-wave simulations of the unit-cells and focal sources. Measurements have been carried out in the CEA-Leti far-field anechoic chamber.

The theoretical directivity of the uniform $7\lambda_0 \times 7\lambda_0$ radiating aperture is equal to 27.9 dBi. This value has been used to compute the TA aperture efficiency.

A. Performance at Broadside

The theoretical (*in-house* tool), simulated (Ansys HFSS) and measured gain at broadside is plotted in Fig. 5 as a function of frequency. The theoretical and simulated results, indicated as 'Nominal' in this Figure, are in a relatively good agreement, with a maximum difference of 1 dB. The theoretical and measured 3 dB gain fractional bandwidths are equal to 14.8% (26.7-31 GHz) and 16.2% (26.2-30.9 GHz) at 29 GHz, respectively. However, significant discrepancies (around 3.4 dB at 29 GHz) have been obtained when comparing simulations and measurements (measured gain: 19.8 dBi, theoretical gain: 23.2 dBi).

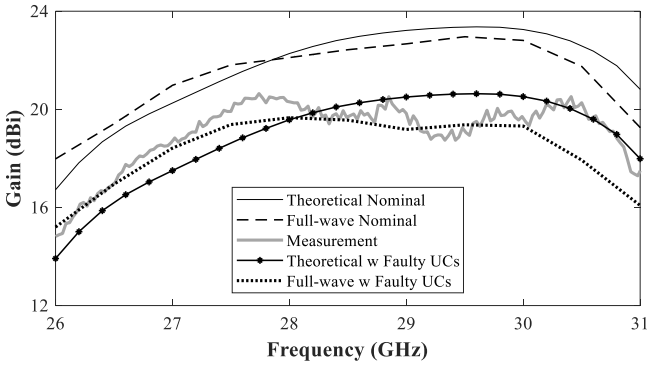

Fig. 5. Theoretical, simulated, and measured broadside gain of the TA prototype as a function of frequency.

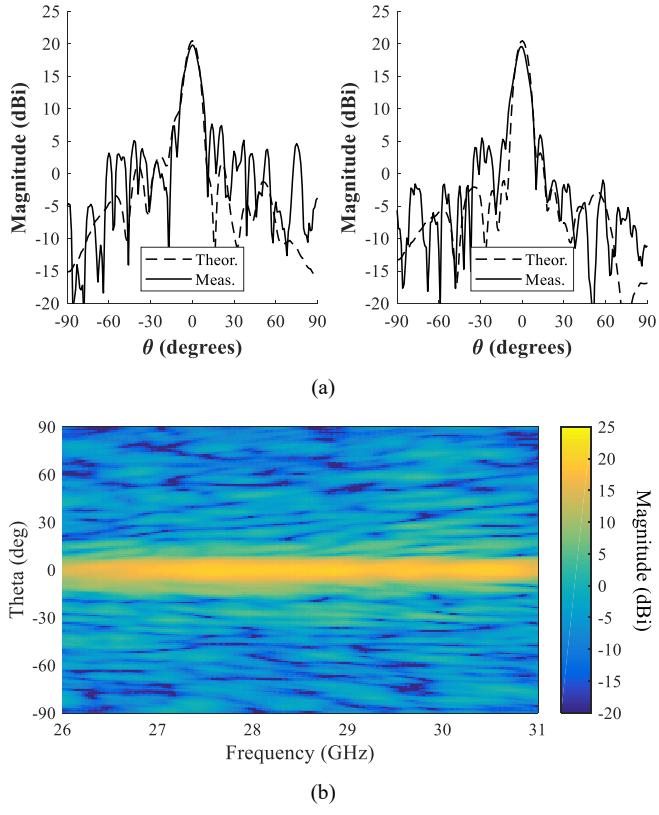

Fig. 6. Radiation characteristics at broadside. (a) Measured and theoretical gain radiation patterns at 29 GHz in E (left) and (right) H planes. (b) Measured gain as a function of frequency and elevation angle in H plane.

To better understand the reasons for these discrepancies, the in-depth diagnostic of the realized prototype has shown that 51 unit-cells were found faulty, most probably due to fabrication defaults in the PCB. DC short circuits between some bias lines and the ground plane have been detected (*e.g.* short circuits between metal layers M2-M3 and M4-M5 most probably generated locally during the PCB pressing and bonding process). The corresponding diodes are thus in the OFF

state. The theoretical and simulated frequency responses, indicated as 'w Faulty UCs', are plotted and compared to measurements and nominal simulations in Fig. 5. They are now in much better agreement with the measurement results, with a maximum gain difference of 0.7 dB at 29 GHz between theory and measurements.

The measured and theoretical gain radiation patterns are plotted and compared in Fig. 6(a) at 29 GHz. It is important to notice that the theoretical results have been calculated by considering in the simulation with the *in-hose* tool the faulty unit-cells. A very satisfactory agreement is obtained for the main lobe in both E and H planes. However, discrepancies on side lobes are observed due to the spill-over and diffraction effects, which are not taken into account in the *in-house* theoretical model. The H-plane radiation patterns measured from 26 to 31 GHz confirms the wide band properties of the antenna (Fig. 6(b)).

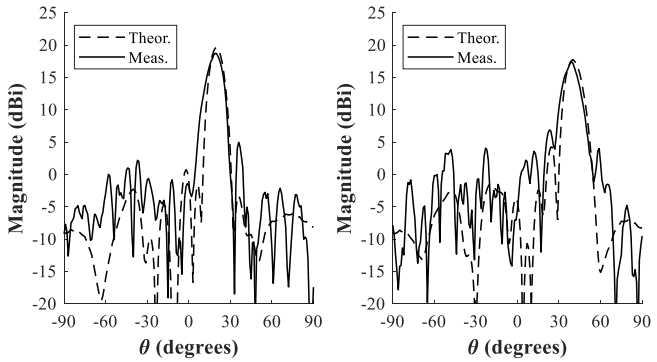

Fig. 7. Scanning radiation characteristics: measured and theoretical gain radiation patterns at 29 GHz in H plane for a steering angle of 20° (left) and 40° (right).

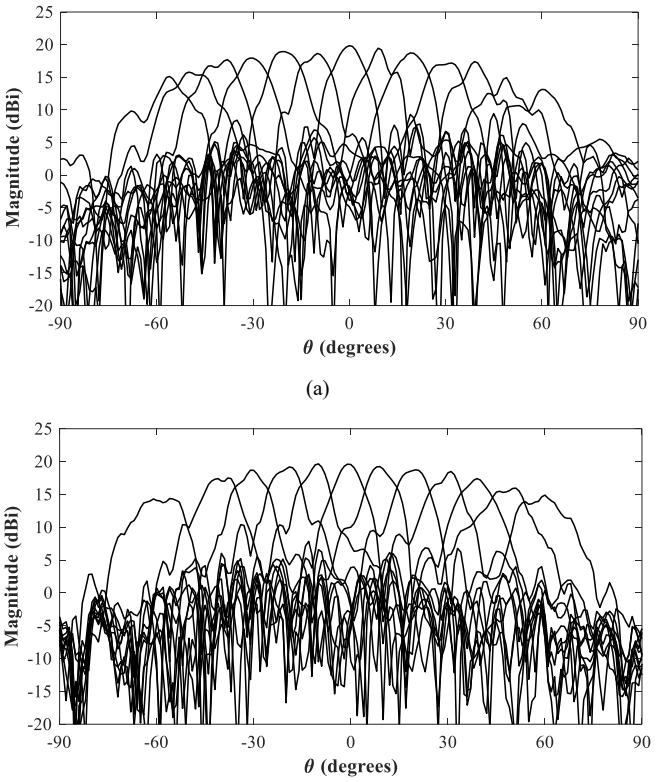

Fig. 8. Measured radiation patterns (realized gain) at 29 GHz as a function of the steering angle. Co-polarization components in (a) E and (b) H planes.

B. *Beam Scanning Performance*

The beam scanning capabilities of the proposed transmitarray have been measured for steering angles between -60° and +60° both in E and H planes.

Fig. 7 represents the measured and theoretical radiation patterns at 29 GHz for an antenna beam pointing at 20° and 40° in H-plane. Experimentally, the corresponding antenna gain reaches 18.7 and 17.4 dBi, respectively. These values are in good agreement with the theory, with a peak gain difference lower than 1 dB. Similar results have been obtained for the other steering angles and H-plane beams.

The scanning capabilities of the antenna are characterized up to 60° in E- and H-planes in Fig. 10(a)-(b). The scan loss at ±60° reaches about 5 dB due to the gain variation of the unit-cell radiation pattern for the same angular range. The slight asymmetry and distortion of the radiation patterns are due to the faulty unit-cells. It is important to notice that symmetrical and non-distorted patterns have been obtained in simulations when the nominal transmitarray configuration without faulty unit-cells is considered. The cross-polarization discrimination is also excellent, with a maximum cross-polarization level lower than 4 dBi between -60° and +60°.

In order to highlight the impact of the 51 faulty unit-cells on the radiation performance of the proposed antenna, the theoretical co-polarization gain patterns have been plotted in Fig. 9. These patterns have been computed at broadside and for different scanning angles in the vertical, horizontal and diagonal planes, when the nominal layout of the transmitarray without faulty unit-cells is considered. These results demonstrate an excellent scanning capability up to 60° and confirm that the pattern asymmetry and distortions are due to the faulty unit-cells.

Finally, the obtained results of the 2-bit electronically steerable transmitarray antenna are summarized and compared to the current state-of-the-art in Table II. As discussed in the Section I, only two prototypes [12],[17] have been done previously at Ka-band. Both prototypes demonstrate an aperture efficiency lower than the one achieved in this work.

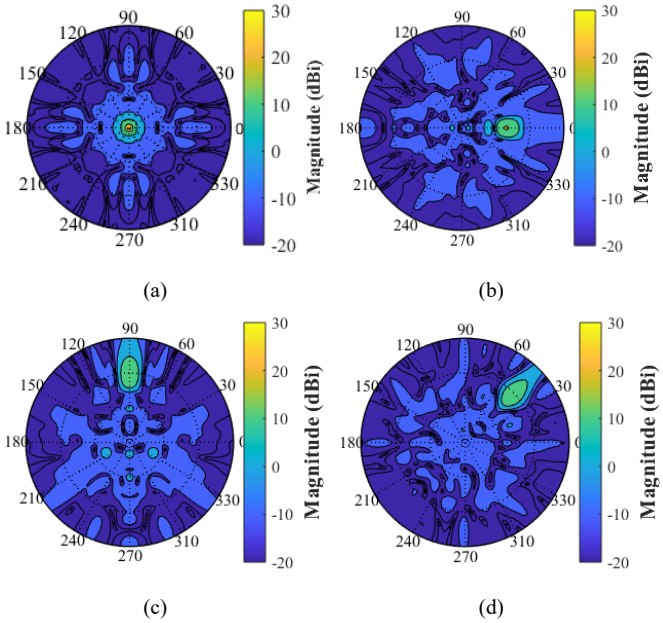

Fig. 9. Theoretical 2-D gain radiation patterns (Ludwig 3 co-polarization component) of the 2-bit steerable transmitarray achieved at 29 GHz when the nominal array layout without faulty unit-cells is considered. (a) Broadside, (b) $(\theta_0,\phi_0) = (40°,0°)$, (c) $(\theta_0,\phi_0) = (60°,90°)$, and (d) $(\theta_0,\phi_0) = (60°,45°)$.

IV. Conclusions

A 2-bit electronically steerable 14×14 element transmitarray has been presented in detail at Ka-band. The proposed antenna is based on a reconfigurable unit-cell with 4 p-i-n diodes to control electronically its transmission phase. Despite some non-operating unit-cells, which is a positive outcome from the application point of view showing the graceful degradation of the performance in such operating conditions, the radiation patterns remain relatively good with moderate side-lobe levels. It is believed that this work represents a significant progress in the current state-of-the-art since there is no other example of a 2-bit active Ka-band transmitarray with such promising results.

The measured aperture efficiency and 3-dB gain fractional bandwidth are equal to 15.9% (35% in simulation) and 16.2% at 29 GHz, respectively.

TABLE II
Performance Comparison With Existing Electronically Steerable Transmitarrays

Reference	[13]	[18]	[12]	[17]	This work
Layers	7	4	4	3	6
Phase shifters	Varactor diodes	p-i-n diodes	p-i-n diodes	MEMS	p-i-n diodes
Freq. (GHz)	4.8	9.8	29.0	34.8	29.0
Polarization	LP	LP	CP	LP	LP
F/D	0.3	0.7	0.6	-	0.67
Phase resolution	400°	1-bit	1-bit	2-bit	2-bit
Gain (dBi)	15.6	22.7	20.8	9.2	19.8
Ap. eff. (%)	34.0	16.0	9.5	6.2	15.9
3-dB BW (%)	9% (2-dB BW)	15.8	14.6	-	16.2
Beam scanning capability	±45° E-, and H-planes	±40°/±60° E-, and H-planes	±60° E-, and H-planes	±40° E-, and H-planes	±60° E-, and H-planes*

* Distortion on the radiation patterns observed for scan angles higher than 40° are due to the faulty unit-cells.

References

[1] S. Raman, R. Weigel, and T. Lee, "The Internet of Space (IoS): a future backbone for the Internet of Things?," *IEEE Internet of Things Magazine Newsletter*, Mar. 8, 2018.

[2] W. W. Milroy, "Continuous transverse stub element devices and methods of making same," U.S. Patent 5 266 961, Nov. 30, 1993.

[3] M. Ettorre, F. Foglia Manzillo, M. Casaletti, R. Sauleau, L. Le Coq, and N. Capet, "Continuous transverse stub array for Ka-band applications," *IEEE Trans. Antennas Propag.*, vol. 65, no. 12, pp. 7009-7018, Nov. 2015.

[4] B. Tripodi, F. Di Marca, T. Cadili, C. Mollura, F. Di Maggio, and M. Russo, "Ka-band active phased array antenna system for satellite communications on the move terminal," in *Proc. European Conf. Antennas Propag. (EuCAP)*, Rome, Italy, Mar. 2011.

[5] R. A. Stevenson, A. H. Bily, D. Cure, M. Sazegar, and N. Kundtz, "Rethinking wireless communications: advanced antenna design using LCD technology," *SID Symposium Digest of Technical Papers*, vol. 46, no. 1, pp. 827-830, 2015.

[6] Kymeta Website. (2018, Sep.) "mTennaTM and Metamaterials" [Online]. Available: http://www.kymetacorp.com.

[7] I. Wolf, C. Günner, J. Kassner, R. Kulke, and P. Uhlig, "New heights for satellites: LTCC multilayer technology for future satellites," *IEEE Microwave Magazine*, vol. 19, no. 1, pp. 36-47, Jan.-Feb. 2018.

[8] ITU-R, Provisional Final Acts, World Radiocommunication Conference (WRC-15), Nov. 2015.

[9] A. H. Naqvi and S. Lim, "Review of recent phased arrays for millimeter-wave wireless communication," *Sensors (Basel)*, vol. 18, 10 3194, Oct. 2018.

[10] K. Kibaroglu, M. Sayginer, and G. M. Rebeiz, "A low-cost scalable 32-element 28-GHz phase array transceiver for 5G communication links based on a 2 × 2 beamformer flop-chip unit-cell," *IEEE Journal Solid-States Circuits*, vol. 53, no. 5, pp. 1260-1274, May 2018.

[11] B. Yang, Z. Yu, J. Lan, R. Zhang, J. Zhou, and W. Hong, "Digital beamforming-based massive MIMO transceiver for 5G millimeter-wave communications," *IEEE Trans. Microw. Theory Tech.*, vol. 66, no. 7, pp. 3403-3418, Jul. 2018.

[12] L. Di Palma, A. Clemente, L. Dussopt, R. Sauleau, P. Potier, and P. Pouliguen, "Circularly-polarized reconfigurable transmitarray in Ka-band with beam scanning and polarization switching capabilities," *IEEE Trans. Antennas Propag.,* vol. 65, no. 2, pp. 529-540, Feb. 2017.

[13] J. G. Nicholls and S. V. Hum, "Full-space electronic beam-steering transmitarray with integrated leaky-wave feed," *IEEE Trans. Antennas Propag.*, vol. 64, no. 8, pp. 3410-3422, Aug. 2016.

[14] F. Diaby, A. Clemente, K. Pham, R. Sauleau, and L. Dussopt, "Circularly-polarized transmitarray antennas at Ka-band," *IEEE Antennas Wireless Pro*pag. *Lett.*, vol. 17, no. 7, pp. 1204-1208, Jul. 2018.

[15] P. Naseri, S. A. Matos, J. R. Costa, and C. A. Fernandes, "Phase-delay versus phase-rotation cells for circular polarization transmit arrays – application to satellite Ka-band beam steering," *IEEE Trans. Antennas Propag*., vol. 66, no. 3, pp. 1236-1247, Mar. 2018.

[16] L. Dussopt, A. Moknache, J. Säily, A. Lamminen, M. Kaunisto, J. Aurinsalo, T. Bateman, and J. Francey, "A V-band switched-beam lineraly-polarized transmit-array antenna for wireless backhaul applications," *IEEE Trans. Antennas Propag.*, vol. 65, no. 12, pp. 6788-6793, Dec. 2017.

[17] C.-C. Cheng, B. Lakshminarayanan, and A. Abbaspour-Tamijani, "A programmable lens-array antenna with monolithically integrated MEMS switches," *IEEE Trans. Microw. Theory Tech.*, vol. 57, no. 8, pp. 1874–1884, Aug. 2009.

[18] A. Clemente, L. Dussopt, R. Sauleau, P. Potier, and P. Pouliguen, "Wideband 400-element electronically reconfigurable transmitarray in X Band," *IEEE Trans. Antennas Propag.*, vol. 61, no. 10, pp. 5017-5027, Oct. 2013.

[19] C. Huang, W. Pan, and X. Luo, "Low-loss circularly polarized transmitarray for beam steering application," *IEEE Trans. Antennas Propag.*, vol. 64, no. 10, pp. 4471-4476, Oct. 2017.

[20] J. R. Reis, R. F. S. Caldeirinh, A. Hammoudeh, and N. Copner, "Electronically reconfigurable FSS-inspired transmitarray for 2-D beamsteering," *IEEE Trans. Antennas Propag.,* vol. 65, no. 9, pp. 4880–4885, Sep. 2017.

[21] Z.-W. Miao, Z.-C. Hao, G. Q. Luo, L. Gao, J. Wang, X. Wang, and W. Hong, "140 GHz high-gain LTCC-integrated transmit-array antenna using a wideband SIW aperture-coupling phase delay structure," *IEEE Trans. Antennas Propag*., vol. 66, no. 1, pp. 182-190, Jan. 2018.

[22] F. Diaby, A. Clemente, L. Di Palma, L. Dussopt, K. Pham, E. Fourn, and R. Sauleau, "Linearly-polarized electronically reconfigurable transmitarray antenna with 2-bit phase resolution in Ka-band," in *Proc. Int. Conf. Electromagnetics Advanced Applications* (*ICEAA 2017*), Verona, Italy, 11-15 Sep. 2017.

[23] F. Diaby, A. Clemente, L. Di Palma, L. Dussopt, K. Pham, E. Fourn, and R. Sauleau, "Design of a 2-bit unit-cell for electronically reconfigurable transmitarrays at Ka-band," in *Proc. 47th European Microwave Conference* (*EuMW 2017*), Nuremberg, Germany, 10-12, Oct. 2017, pp. 1321-1324.

[24] MACOM technologies, www.macom.com.

[25] L. Di Palma, A. Clemente, L. Dussopt, R. Sauleau, P. Potier, and P. Pouliguen, "1-bit reconfigurable unit-cell for Ka-band transmitarrays," *IEEE Antennas Wireless Propag. Lett,* vol. 15, pp. 560-563, 2016.